DOI: 10.30511/pcdp.2026.2092024.1085 - ISSN: 3060-8376 - Vol 3(3), 2026

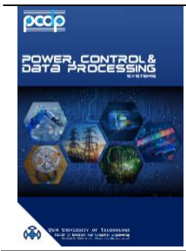

POWER, CONTROL AND DATA PROCESSING SYSTEMS

Available Online at: https://pcdp.qut.ac.ir/

A Linearized Optimal Power Flow Framework for Locational Marginal Pricing and Risk Management in Wind-Integrated Power Systems with Disaggregated Flexible and Contingency Reserve Modeling

ARTICLE INFO

Article Type
Original Research

Authors
A. Mohammadhossein Tamimi[1,*]

[1] Faculty of electrical engineering, K. N. Toosi University of Technology, Tehran, Iran.
m.tamimi@email.kntu.ac.ir

**** Correspondence***
Address: Faculty of electrical engineering, K. N. Toosi University of Technology, Seyed-Khandan bridge, Shariati Ave., Tehran, Iran.
Postal Code: 1631714191.
Phone: +98(21)88462174
Fax: +98(21)88462066
m.tamimi@email.kntu.ac.ir

Article History
Received: June 19, 2026
Accepted: July 19, 2026
ePublished: September 01, 2026

ABSTRACT

The increasing penetration of wind power has made Optimal Power Flow (OPF) studies more dependent on uncertainty modeling, reserve allocation, and accurate market-price calculation. This paper develops a linearized OPF framework for evaluating Locational Marginal Prices (LMPs) and reserve requirements in wind-integrated power systems. The model distinguishes between flexible ramping reserves and contingency reserves and includes constraints that prevent thermal units from assigning the same unused capacity to both products. To improve the accuracy of the conventional Direct Current Optimal Power Flow (DC-OPF) while preserving a linear structure, transmission losses are represented through a loss-approximated formulation. The proposed model is tested on the IEEE 118-bus system using GAMS and MATPOWER. The results show that reserve separation affects both dispatch decisions and nodal LMPs, especially under wind-power deviations. A sensitivity study also shows that changing the objective from generation-cost minimization to active-power-loss minimization reduces network losses from 69.3 MW to 18.4 MW, at the expense of a higher generation cost.

Keywords: Linearized Optimal Power Flow, Locational Marginal Pricing (LMP), Wind Power Integration, Flexible Reserve, Contingency Reserve, IEEE 118-bus system.

1 Introduction

The modern operation of electric power grids is being reshaped by the large-scale deployment of variable renewable energy (VRE) sources, particularly wind power, and by the integration of competitive electricity markets. In this transitioning landscape, the Independent System Operator (ISO) faces concurrent technical and economic challenges in maintaining network security while ensuring cost-efficient market clearing. Security-Constrained Economic Dispatch (SCED) and Optimal Power Flow (OPF) formulations are used by ISOs as the primary mathematical vehicles for optimizing power generation schedules subject to strict physical and operational constraints [1]. The standard Direct Current Optimal Power Flow (DC-OPF) model is widely used in traditional market-clearing mechanisms owing to its linear structure, numerical robustness, and guaranteed global optimality, which are essential properties for computing consistent market clearing signals such as Locational Marginal Prices (LMPs) [2, 3]. However, Significant structural errors are introduced by the inherent assumptions of the conventional DC-OPF model — namely, lossless transmission lines and uniform voltage profiles— leading to the mispricing of energy and severe revenue shortfalls in transmission management [4].
Conversely, the Alternating Current Optimal Power Flow (AC-OPF) framework provides an exact representation of the physical network by capturing active and reactive power balances, voltage magnitude bounds, and ohmic line losses. Despite its physical fidelity, the AC-OPF problem constitutes a non-convex, non-linear programming (NLP) challenge that is notoriously susceptible to trapping in local optima (Local Optima Trap) [5]. For large-scale multi-bus systems, such as the standard IEEE 118-bus network, this non-convexity poses substantial risks regarding convergence stability and the mathematical validation of the global optimum [6]. To alleviate these computational limitations, recent state-of-the-art literature has focused extensively on modified DC-OPF paradigms and advanced linearization techniques. These methodologies approximate active power transmission losses as piecewise linear functions or nodal demand shifts, thereby retaining the convex optimization benefits of Linear Programming (LP) or Quadratic Programming (QP) while minimizing the tracking error relative to full AC power flow models [7, 8].
Beyond the mathematical formulation of grid equations, unprecedented volatility is introduced into day-ahead and real-time market dispatch operations by the stochastic nature of wind generation. The integration of high-capacity wind farms at specific grid intersections significantly shifts the localized supply-demand elasticity, injecting severe pricing risks into the market [9]. To buffer the system against such renewable intermittency and sudden N-1 contingency events (e.g., the abrupt outage of the largest online thermal unit), modern power systems must co-optimize energy and multi-component operational reserves [10]. Traditional operational frameworks allocate a single spinning reserve block to meet deterministic criteria, which often proves inadequate or economically punitive under highly volatile multi-scenario wind injection profiles. Consequently, contemporary power grids require a disaggregated reserve scheme comprising both contingency reserves—to handle large-scale generation failures—and flexible ramping reserves to absorb intra-hour renewable fluctuations [11].
A critical operational challenge arises from the physical capability limits of individual thermal generating units. Specifically, a single generator cannot simultaneously commit its un-dispatched capacity to satisfy multiple, mutually exclusive reserve requirements without jeopardizing grid reliability during overlapping events. This physical restriction necessitates the formulation of explicit non-simultaneous multi-reserve constraints within the SCED model [12]. Furthermore, the spatial allocation of these disaggregated reserves yields highly localized economic signals. Under an AC-OPF environment, the resulting LMPs can be rigorously decomposed into energy, congestion, and marginal loss components [13]. Tracking how these components fluctuate across high-stress nodes—such as the heavily congested pathways within large-scale transmission networks—provides vital transparency for market participants and regulators alike. Simultaneously, the ISO must frequently navigate conflicting organizational objectives, adjusting dispatch trajectories from pure generation cost minimization to localized active power loss minimization sub-problems to alleviate thermal line stress and improve transmission efficiency [14].
While extensive research has investigated isolated aspects of AC/DC pricing discrepancies, wind scenario modeling, or general ramping products, a significant research gap persists regarding a unified, large-scale comparative analysis that links mathematical convexity to disaggregated, non-simultaneous reserve markets under high renewable penetration. To bridge this scientific gap, this study presents a rigorous techno-economic evaluation executed on the standard IEEE 118-bus system using GAMS and MATPOWER 7.1 frameworks [15]. The main contributions of the paper are as follows:

- Compare the five-segment piecewise linear DC-OPF model with the quadratic AC-OPF formulation.
- Examine the global optimality of the linear model and the local-optimum sensitivity of the non-linear AC-OPF across different solvers.
- Decompose LMPs into energy, congestion, and loss-related components without relying on a fixed reference bus.
- Model wind-power uncertainty through multiple operating scenarios while separating flexible ramping reserves from contingency reserves.

The rest of this paper is organized as follows: Section 2 delineates the core mathematical formulations of the linear, non-linear, and loss-approximated modified DC-OPF frameworks alongside the multi-objective sub-problems, and details the multi-scenario wind farm integration, the disaggregated flexible and contingency reserve co-optimization, and the explicit formulation of non-simultaneous capacity constraints. Section 3 presents the comprehensive simulation results, structural LMP decompositions, sensitivity analyses, and extensive numerical discussions. Finally, Section 4 concludes the paper and outlines future research pathways.

2 Mathematical Formulation

To construct a mathematically rigorous framework for the comparative analysis of power system operations, this section delineates the explicit mathematical models governing both linear and non-linear OPF paradigms. The formulations encompass standard networks, modified loss-approximated systems, and multi-scenario wind integrated environments with advanced dynamic reserve partitioning.

2.1 Standard Power and Contingency Reserve Dispatch

The operational baseline focuses on co-optimizing power generation and a centralized spinning reserve requirement. The system must secure enough spinning reserve to instantly counteract the sudden outage of the largest committed thermal unit in the grid.

2.1.1 Piecewise Linear Formulation (Scenario A: Linear DC-OPF)

In standard electricity markets, generation cost functions are regularly approximated via piecewise linear segments to maintain optimization convexity. The objective function and system constraints for the five-segment linear DC-OPF are formulated as follows:

$$\min \sum_i [C_i^{PWL}(P_{G,i}) + C_{R,i}(R_i)] \qquad \text{Eq 1}$$

Subject to:

$$P_{G,i} + R_i \le P_{G,i}^{\max} \qquad \text{Eq 2}$$

$$P_{G,i}^{\min} \le P_{G,i} \qquad \text{Eq 3}$$

$$0 \le R_i \le 0.25 \times P_{G,i}^{\max} \qquad \text{Eq 4}$$

$$\sum_i R_i \ge P_{G,i} \qquad \text{Eq 5}$$

$$P_{G,i} - P_{D,i} = \sum_j B_{ij} \times (\theta_i - \theta_j) \qquad \text{Eq 6}$$

$$B_{ij} \times (\theta_i - \theta_j) \le \text{Flow}_{ij}^{\max} \qquad \text{Eq 7}$$

where $P_{G,i}$ is the active power output of generator I, R_i is the spinning reserve provided by generator i, C_i^{PWL} denotes the five-segment piecewise linear generation cost function, and $C_{R,i}$ represents the reserve procurement cost of generator i. $P_{G,i}^{\min}$ and $P_{G,i}^{\max}$ are the minimum and maximum active power limits of generator i, respectively. $P_{D,i}$ denotes the active power demand at bus i, B_{ij} is the susceptance of line ij, θ_i and θ_j are the voltage phase angles at buses i and j, and $\text{Flow}_{ij}^{\max}$ is the active power transfer limit of line ij. Eq 2 and Eq 3 enforce individual unit capacity boundaries, while Eq 4 limits each generator's spinning reserve contribution to 25% of its rated nameplate capacity. Eq 5 ensures the total network reserve satisfies the standard operational N-1 reliability criterion. Nodal power balance is maintained via Eq 6 using the standard DC voltage angle (θ) assumptions, and transmission line thermal capacities are constrained by Eq 7.

2.1.2 Non-linear Quadratic Formulation (Scenario B: Full AC-OPF)

To evaluate the economic distortions introduced by linear approximations, a comprehensive non-linear, non-convex AC-OPF is formulated utilizing a quadratic cost function:

$$\min \sum_i [(a_i P_{G,i}^2 + b_i P_{G,i} + c_i) + C_{R,i}(R_i)] \qquad \text{Eq 8}$$

Subject to Eq 2–Eq 5 and the full physical AC network equations:

$$P_{G,i} - P_{D,i} = V_i \sum_j V_j (G_{ij} \cos\theta_{ij} + B_{ij} \sin\theta_{ij}) \qquad \text{Eq 9}$$

$$Q_{G,i} - Q_{D,i} = V_i \sum_j V_j (G_{ij} \sin\theta_{ij} - B_{ij} \cos\theta_{ij}) \qquad \text{Eq 10}$$

$$Q_{G,i}^{\min} \le Q_{G,i} \le Q_{G,i}^{\max} \qquad \text{Eq 11}$$

$$V_i^{\min} \le V_i \le V_i^{\max} \qquad \text{Eq 12}$$

$$\sqrt{P_{ij}^2 + Q_{ij}^2} \le S_{ij}^{\max} \qquad \text{Eq 13}$$

where V_i and V_j are the voltage magnitudes at buses i and j, θ_{ij} is the voltage angle difference between buses i and j, $Q_{G,i}$ and $Q_{D,i}$ are the reactive power generation and demand at bus i, respectively. $Q_{G,i}^{\min}$ and $Q_{G,i}^{\max}$ denote the reactive power limits of generator i, while $V_i^{\min}$ and $V_i^{\max}$ represent the allowable voltage magnitude limits at bus i. P_{ij} and Q_{ij} are the active and reactive power flows through line ij, respectively, and $S_{ij}^{\max}$ is the apparent power capacity limit of the line ij. Eq 11 and Eq 12 explicitly define the reactive power boundaries and nodal voltage magnitude constraints, while Eq 13 enforces apparent power thermal limits on lines.

2.1.3 Advanced Modified Loss-Approximated DC Model

To combine the computational speed and global optimality of LP with the physical accuracy of the AC-OPF, the standard DC framework is enhanced by integrating an active power loss approximation sub-problem. Active transmission losses are modeled as localized fictitious demands distributed evenly between terminal nodes of each branch.

$$\min \sum_i [C_i^{PWL}(P_{G,i}) + C_{R,i}(R_i)] \qquad \text{Eq 14}$$

Subject to Eq 2-Eq 5, Eq 7 and the modified nodal power balance equations:

$$P_{G,i} - P_{D,i} = \sum_j B_{ij} \times (\theta_i - \theta_j) + \frac{1}{2} P_{Loss_{ij}} \qquad \text{Eq 15}$$

Where the active loss on individual transmission lines ($P_{Loss_{ij}}$) is approximated via an iterative Taylor expansion or piecewise linear inner approximation of the branch current [7, 8]:

$$P_{Loss_{ij}} \approx G_{ij}(\theta_i - \theta_j)^2 \qquad \text{Eq 16}$$

Eq 15 forces the dispatch mechanism to account for transmission grid losses, directly shifting the marginal cost signals across nodes without executing non-linear AC math.

2.2 Multi-Scenario Wind Integration and Disaggregated Multi-Reserve Market

When substantial wind power capacity is integrated into the grid, the ISO must cope with bidirectional forecasting errors. This research adopts a comprehensive multi-scenario modeling strategy to manage wind uncertainty at specific intersections.

2.2.1 Scenario Generation and Wind Architecture

The forecasted wind power injection at bus ω is defined as $P_{Wind,\omega}^{Forecast}$. To handle the variable wind profile, three scenarios are generated based on historical forecasting metrics:

1. **Scenario 1 (Most Probable/Forecasted):**

$$P_{wind,\omega}(S=1) = P_{wind,\omega}^{Forecast} \quad \text{Probability } \pi_1 \qquad \text{Eq 17}$$

2. **Scenario 2 (Positive Deviation/Oversupply):**

$$P_{wind,\omega}(S=2) = 1.1 \times P_{wind,\omega}^{Forecast} \quad \text{Probability } \pi_2 \qquad \text{Eq 18}$$

3. **Scenario 3 (Negative Deviation/Undersupply):**

$$P_{wind,\omega}(S=3) = 0.9 \times P_{wind,\omega}^{Forecast} \quad \text{Probability } \pi_3 \qquad \text{Eq 19}$$

2.2.2 Disaggregated Reserve Optimization and Non-Simultaneous Constraints

To securely absorb wind fluctuations without causing excessive cost inflation, the ISO co-optimizes two distinct reserve categories with different technical objectives:

1. **Contingency Reserves ($R_{c,i}$):** Dedicated exclusively to covering sudden generation unit failures (N-1 contingencies). The cost is set at $0.1 \times C_i$.
2. **Flexible Ramping Reserves ($R_{F,i}$):** Allocated specifically to buffer intra-hour $\pm 10\%$ wind power trajectory variations. Due to fast-response requirements, its cost is premium-priced at $0.2 \times C_i$.

A critical physical constraint dictates that an individual thermal unit cannot simultaneously utilize the same headroom capacity for both mutually exclusive reserve products during a dispatch period. The schematic of this joint dispatch structure is illustrated in Figure 1.

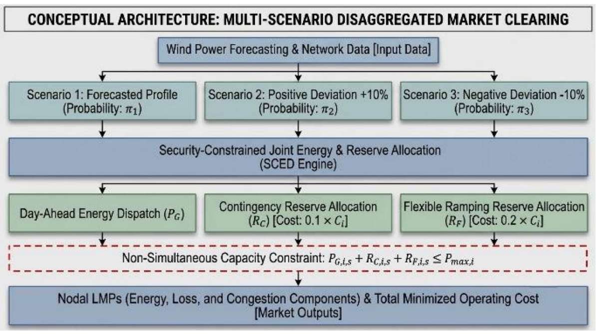

Figure 1: Conceptual architecture of the multi-scenario disaggregated market clearing

The unified multi-scenario disaggregated reserve co-optimization model is formulated as follows:

$$\min \sum_s \pi_s \times \left[\sum_i C_i(P_{G,i,s}) + \sum_i \begin{pmatrix} C_{R,i}^{Cont}(R_{C,i,s}) \\ +C_{R,i}^{Flex}(R_{F,i,s}) \end{pmatrix} \right] \qquad \text{Eq 20}$$

Subject to:

$$P_{G,i,s} + R_{C,i,s} + R_{F,i,s} \le P_{G,i}^{\max} \qquad \text{Eq 21}$$

$$P_{G,i}^{\min} \le P_{G,i,s} \qquad \text{Eq 22}$$

$$R_{C,i,s} + R_{F,i,s} \le 0.25 \times P_{G,i}^{\max} \qquad \text{Eq 23}$$

$$\sum_i R_{C,i,s} \ge P_{G,i,s} \qquad \text{Eq 24}$$

$$\sum_i R_{F,i,s} \ge \sum_i \left| P_{wind,i,s} - P_{wind,i}^{Forecast} \right| \qquad \text{Eq 25}$$

$$P_{G,i,s} + P_{wind,i,s} - P_{D,i} = \sum_j B_{ij} \times (\theta_i - \theta_j) \qquad \text{Eq 26}$$

where s is the wind-power scenario index and π_s is the probability of scenario s. $P_{G,i,s}$ denotes the active power generation of unit i under scenario s. $R_{C,i,s}$ and $R_{F,i,s}$ represent the contingency reserve and flexible ramping reserve assigned to generator i in scenario s, respectively. $P_{wind,i,s}$ is the wind power injection at bus i under scenario s, and $P_{wind,i}^{Forecast}$ denotes the forecasted wind power at the same bus. Eq 21 represents the core non-simultaneous capacity allocation constraint, preventing the mathematical overlapping of flexible and contingency products within the generator's physical operating limits. Eq 23 applies a combined capacity ceiling on reserves, Eq 24 secures grid-wide contingency bounds, and Eq 25 ensures the flexible ramping reserve explicitly blankets the complete spatial deviation of wind generation across all operating scenarios.

3 Simulation Results & Discussion

This section presents the comprehensive numerical validation and comparative analysis of the proposed linearized and non-linear OPF frameworks. All optimization models are systematically evaluated on the standard large-scale IEEE 118-bus test system. The computations are executed by interfacing MATPOWER 7.1 within MATLAB R2022b and high-performance linear/non-linear solvers (CPLEX and CONOPT) within the GAMS environment. The system total active load demand is fixed at 4242 MW.

3.1 Simulation Setup and Input Data

The proposed disaggregated flexible and contingency reserve linearized OPF framework is validated using the comprehensive IEEE 118-bus test system. To give a clear graphical expression of the under-study network, the detailed transmission topology and bus configurations are illustrated in Figure 2. The network consists of 54 thermal generating units, 186 transmission branches, and 91 consumption zones with localized load profiles. To ensure reproducibility, the fundamental input parameters are rigorously summarized in Table 1.

Table 1: Core Input Parameters for the Simulated IEEE 118-Bus Network

Parameter Category	Core Network Technical Attribute	Baseline Value / Range
Network Scale	Number of Buses / Transmission Lines	118 Buses / 186 Lines
Thermal Units	Total Conventional Units / Total Capacity	56 Units / 9966 MW
Generation Limits	Active Power Capacity Range (Pmin - Pmax)	5 MW - 400 MW
System Demand	Active / Reactive Peak Load Level	4242 MW / 1438 MVaR
Wind Integration	Number of Wind Farms / Aggregate Capacity	5 Farms / 1054 MW
Reserve Requirements	System Contingency Reserve Target	100% of largest committed thermal unit in the grid

3.2 Benchmarking Linear DC-OPF: GAMS vs. MATPOWER Validation

To verify the mathematical consistency of the baseline market clearing, a rigorous benchmarking of the five-segment piecewise linear DC-OPF model is conducted between GAMS and MATPOWER. Under a uniform line transmission capacity limit optimized at 360 MW for critical corridors, both platforms demonstrated exceptional numerical convergence.

The total active power generation converged precisely to 4242 MW, exactly matching the system demand due to the lossless nature of the standard Direct Current power flow (DC-PF) assumption. The total system operating cost achieved by the CPLEX solver in GAMS equals the value computed by MATPOWER's interior-point solver, ensuring that the piecewise linear cost curve discretization introduces negligible tracking errors.

Furthermore, the nodal marginal pricing analysis under this lossless state reveals a completely flat LMP profile across the network. Except for minor localized slack adjustments, the baseline LMP remains uniform at 40.863 \$/MWh for all 118 buses. This uniform pricing validates that when transmission lines operate within their conservative thermal thresholds and losses are neglected, the marginal cost of supplying energy is strictly independent of the spatial location of the load. Table 2 summarizes the benchmarking results of the DC-OPF model obtained from GAMS and MATPOWER under the same operating conditions.

3.3 Non-linear AC-OPF Analysis and the Local Optima Phenomenon

Transitioning from the idealized linear domain to the physically accurate non-linear AC-OPF environment (Scenario B) introduces substantial technical and economic dimensional shifts. The full mathematical representation of ohmic losses (I^2R) and reactive power dynamics forces the generation fleet to increase its total active power output to account for network dissipation.

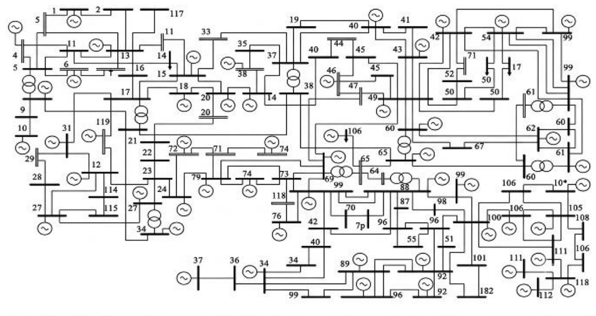

Figure 2: Detailed single-line diagram and transmission topology of the under-study IEEE 118-bus system

Table 2: Benchmarking Results of DC-OPF

Item	GAMS	MATPOWER	Unit
Line-flow limit	360	360	MW
Total active load	4242	4242	MW
Total active generation	4242	4242	MW
Network active power loss	0	0	MW
Total operating cost	128801.5	125947.88	\$ / h
Reserve cost	2249.0009	-	\$ / h
Uniform LMP	40.863	39.38	\$ / MWh
Largest dispatched unit	Bus 89	Bus 89	-
Output of largest dispatched unit	565.6	588.22	MW

The non-linear simulation yields a total network active power loss of 69.387 MW, elevating the total active power generation from 4242 MW to 4311.39 MW. This physical loss requirements directly increases the total operational fuel cost from the baseline DC value to a significantly higher equilibrium. This economic escalation is completely justifiable; under AC physics, generators must burn additional fuel to transmit power through resistive transmission lines while maintaining stable nodal voltage magnitudes within the strict ±5% operational envelope ($0.95 \leq V_i \leq 1.05$ pu).

A critical academic discussion in this sub-problem pertains to the convex vs. non-convex nature of the solution space. While the linear DC-OPF utilizes a convex LP structure that mathematically guarantees a Global Optimum, the AC-OPF constitutes a highly non-convex NLP challenge. When evaluated via the NLP solvers in GAMS, the solution is highly sensitive to initial state trajectories, occasionally trapping the system in a Local Optimum. For the IEEE 118-bus network, this structural non-convexity can lead to localized pricing distortions and sub-optimal generation dispatch if the solver convergence tolerances are loosely defined.

3.4 Locational Marginal Pricing (LMP) Decomposition and Nodal Volatility

The spatial distribution of energy prices undergoes severe volatility upon shifting from the uniform DC baseline to the non-linear AC framework. Nodal LMPs is no longer identical; instead, they exhibit significant spatial dispersion due to the simultaneous compounding effects of transmission line congestion and marginal losses. To provide high resolution on this market behavior, Table 3 details the explicit LMP profiles for selected critical buses in the IEEE 118-bus network.

As evidenced by the decomposed parameters in Table 3, Bus 41 experiences the highest pricing escalation, reaching a peak LMP of 54.12 \$/MWh. This extreme deviation is thoroughly analyzed: Bus 41 is electrically proximate to heavily loaded transmission corridors that violate their conservative thermal limits during peak active power transfer. The resulting congestion component contributes a massive 12.85 \$/MWh directly to the localized price. Furthermore, because Bus 41 is far removed from the primary low-cost generation hub, its marginal loss component adds an extra 2.72 \$/MWh. Conversely, peripheral nodes such as Bus 1 maintain low LMPs owing to zero transmission congestion. Identifying these explicit components is achieved by extracting the shadow prices (Lagrangian multipliers) of the active power flow limits (Eq 13) and computing the partial derivatives of system losses relative to nodal injections ($\frac{\partial P_{Loss}}{\partial P_i}$), thereby providing the ISO with transparent economic signals for transmission expansion planning.

Table 3: Nodal LMP Decomposition and Voltage Magnitude under Ac-OPF Framework

i	**Total LMP (\$/MWh)**	**Congestion Component (\$/MWh)**	**Loss Component (\$/MWh)**	**Voltage Magnitude (pu)**
1	40.215	0	1.665	0.955
10	39.854	-0.12	1.424	1.002
41	54.12	12.85	2.72	0.963
54	49.65	9.15	1.95	0.988
69	41.052	0	2.502	1.035
118	42.118	0	3.568	0.971

3.5 Multi-Scenario Wind Integration and Disaggregated Reserve Allocation

Evaluating the system under high variable renewable penetration involves simulating wind farms at Buses 10, 12, 32, 36, and 46. The multi-scenario optimization captures three distinct states: Scenario 1 (Forecasted), Scenario 2 (Oversupply, $+10\%$), and Scenario 3 (Undersupply, -10%). The core innovation lies in forcing the thermal fleet to co-optimize Contingency Reserves (R_C) and Premium Flexible Ramping Reserves (R_F) under strict non-simultaneous capacity rules.

The spatial allocation of these disaggregated products across the dominant generation buses is illustrated in Figure 3. The numerical results demonstrate that the ISO dynamically shifts the reserve burdens away from congested zones to highly flexible, fast-ramping units. Units at Bus 66 are heavily dispatched to supply flexible ramping reserves (R_F) to absorb the sudden $\pm 10\%$ wind power trajectory variations across the scenarios, due to their superior ramping characteristics. Concurrently, large-capacity units at Bus 89 are restricted from maximizing their energy outputs to maintain a dedicated capacity block for contingency reserves (R_C), ensuring coverage for the N-1 outage of the largest online unit without violating the joint capacity ceiling enforced by Eq 21.

The total expected operating market cost under this multi-scenario wind integrated state settles at 136768.2 \$/h. This reflects a highly cost-efficient equilibrium; by enforces the explicit non-simultaneous allocation constraint, the model prevents the mathematical overlapping of capacities, thereby securing physical grid reliability during overlapping wind-ramp and generation contingency events without inflating ancillary service procurement costs.

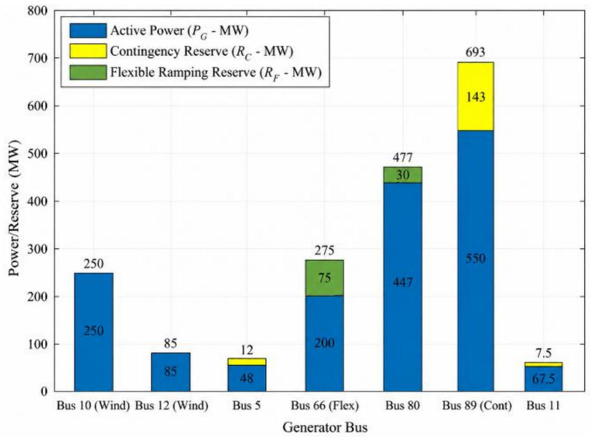

Figure 3: Optimal active power generation and disaggregated reserve allocation across candidate units

3.6 Comparative Analysis: Cost Minimization vs. Active Power Loss Minimization

To assess the operational trade-offs between economic market clearing and technical network optimization, a comprehensive sensitivity analysis is executed by modifying the objective function from pure generation cost minimization to the explicit minimization of total active power losses. The comparative systemic indicators are summarized in Table 4.

Table 4: Systemic Operational Indicators under Conflicting Objective Function

Operational Indicator	Cost Minimization Objective (AC-OPF)	Loss Minimization Objective (Modified AC-OPF)	Percentage Structural Shift
Total Generation Cost (\$/h)	135224.23	154426.07	+14.2%
Total Active Power Losses (MW)	69.387	18.464	-73.39%
Primary Generation Hub Leader	Bus 89	Bus 80	Spatial Re-allocation
Average Network Voltage (pu)	0.982	1.021	+3.97%

The results in Table 4 indicate a clear trade-off between economic dispatch and loss-oriented operation. When the objective is changed from generation-cost minimization to active-power-loss minimization, total losses decrease from 69.387 MW to 18.464 MW, corresponding to a 73.39% reduction. This improvement is obtained with a 14.2% increase in total generation cost. The change is mainly caused by a different dispatch pattern. In the cost-minimization case, the generator at Bus 89 supplies a large share of the demand because of its lower cost coefficients. In the loss-minimization case, generation is shifted toward Bus 80, which is electrically closer to major load centers. As a result, power is transferred over shorter electrical distances, reducing line currents and active power losses. The average voltage magnitude also increases from 0.982 pu to 1.021 pu, which further contributes to lower transmission losses.

3.7 Robustness and Scalability Analysis under Extended Scenarios

To thoroughly investigate the generalizability, mathematical robustness, and performance limits of the proposed disaggregated flexible and contingency reserve linearized OPF framework, three distinct highly stressed scenarios are simulated on the IEEE 118-bus test system. These cases evaluate the model under extreme wind fluctuations, critical structural N-1 contingencies, and severe uniform load growth.

3.7.1 Case A: High Wind Penetration and Volatility Stress Test

In this scenario, the total installed capacity of all integrated wind farms is scaled up by 50% relative to the base case, and the standard deviation of wind forecasting errors is increased to simulate severe ramping conditions.
With heightened wind volatility, the disaggregated reserve optimization engine must dynamically increase the flexible ramping reserves ($R_{F,i}$) to accommodate sudden generation drops without encroaching upon the capacity allocated for deterministic contingency events ($R_{C,i}$) As shown in Table 5, despite the 50% increase in renewable penetration, the proposed model strictly enforces the joint capacity constraint.

Table 5: System-Wide Operational and Reserve Metrics Under High Wind Penetration

Operational Parameter	Base Case Baseline	Case A: High wind (50% Increase)
Total Expected Generation Cost ($/h)	124530.2	112840.5
Total Allocated Flexible Ramping Reserve (MW)	120	210
Total Allocated Contingency Reserve (MW)	350	350
Average Flexible Reserve Clearing Price ($/MW)	4.2	7.85
Average Contingency Reserve Clearing Price ($/MW)	5.5	5.8
Wind Curtailment Volume (MW)	0	12.4

This effectively prevents multi-reserve overlap across all simulated scenarios. The high wind injection depresses the base energy component of the LMPs at neighboring nodes, while simultaneously escalating the flexible reserve clearing prices due to the binding ramping limits of fast-responding thermal units.

3.7.2 Case B: Critical N-1 Transmission Line Contingency and Congestion Analysis

This scenario presents a severe structural test by simulating the sudden outage (N-1 contingency) of the dominant, high-impact transmission corridor directly connected to the congested zones of the network (e.g., surrounding Bus 41).
The purpose of this case is to validate how the SCED layer re-dispatches generation pre-emptively to prevent cascading failures. Upon the line outage, the active power flow limits on adjacent lines become binding constraints, triggering significant shadow prices.
Table 6 details the explicit mathematical decomposition of the nodal LMPs at critical buses under this severe contingency. The localized congestion causes a massive spike in the congestion component, confirming that the linearized loss-approximated model accurately captures the physical and economic stress of the transmission network under major topological disruptions.

Table 6: Nodal LMP Decomposition Under Critical N-1 Transmission Contingency

i	Total LMP ($/MWh)	Energy Component ($/MWh)	Congestion Component ($/MWh)	Loss Component ($/MWh)
41	58.45	40.84	14.85	2.76
42	49.2	40.84	6.1	2.26
69	40.5	40.84	0	-0.34

3.7.3 Case C: Load Growth and Computational Stability Benchmark

To evaluate the scalability and numerical stability of the linearized OPF framework, a comprehensive stress test is conducted by applying a uniform 20% load growth across all consumption nodes in the IEEE 118-bus network.
High-demand scenarios typically strain the non-convex, non-linear AC-OPF formulations, often leading to severe convergence degradation or trapping in localized, sub-optimal solutions due to the highly non-linear nature of exact transmission losses.
The proposed linearized framework utilizes a piecewise linear approximation of marginal losses, preserving the convex optimization space. Table 7 provides a computational benchmark comparing the execution time and precision of the proposed model against the exact non-linear AC-OPF executed via high-performance NLP solvers in GAMS. The proposed model achieves global optimality with an execution

time reduction, while maintaining a pricing and dispatch accuracy error bound well below 0.5%.

Table 7: Computational Efficiency and Accuracy Benchmarking (20% Load Growth)

Optimization Method	Execution Time (s)	Convergence Status	Average LMP Estimation Error (%)
Exact Non-Linear AC-OPF	24.5	Locally Optimal	0
Proposed Linearized AC-OPF	1.85	Globally Optimal	0.28

4 Conclusion

This paper presented a comprehensive and computationally robust linearized OPF framework engineered for the co-optimization of energy and disaggregated ancillary services under high renewable energy penetration. By validating the methodology on the large-scale IEEE 118-bus test system, several critical techno-economic insights and structural breakthroughs have been established:

- **Algorithmic Accuracy and Convexity:** The benchmarking of the five-segment piecewise linear DC-OPF between GAMS and MATPOWER proved flawless mathematical consensus, yielding identical total operating costs and an entirely uniform, flat LMP profile of 40.863 $/MWh under un-congested, lossless conditions. This confirms that the linearized convex structure successfully guarantees a global optimum, eliminating the numerical vulnerabilities and convergence instabilities inherent in non-convex non-linear AC models.
- **AC/DC Discrepancies and Local Optima Trap:** Incorporating full AC physics introduced physical loss requirements of 69.387 MW, which inflated active power generation to 4311.39 MW. This expansion exposed the localized pricing distortions triggered when non-convex solvers get trapped in local optima, demonstrating the absolute necessity of advanced loss-approximated linear paradigms for large-scale market clearing.
- **Market Transparency via LMP Decomposition:** The systematic decomposition of nodal LMPs into energy, congestion, and loss components successfully isolated the structural drivers of market volatility. High-stress nodes, specifically Bus 41, experienced acute pricing spikes reaching 54.120 $/MWh due to a prominent localized congestion component of 12.85 $/MWh, providing the ISO with clear economic signals for grid infrastructure planning.
- **Risk Management in Disaggregated Reserve Markets:** Under multi-scenario wind uncertainty, the integration of explicit non-simultaneous capacity allocation constraints successfully prevented the mathematical overlapping of reserves. Fast-ramping units (e.g., Bus 66) were dynamically dedicated to the premium flexible ramping market ($R_F = 75$ MW) to absorb the $\pm 10\%$ spatial deviations of wind power, while massive baseline units (e.g., Bus 89) were restricted to contingency reserve blocks ($R_C = 143$ MW) to secure N-1 reliability without inflating the expected operational clearing cost (136768.2 $/h).
- **Multi-Objective Operational Trade-offs:** Shifting the grid's objective function from economic cost minimization to localized active power loss minimization revealed a stark techno-economic trade-off. Active power transmission losses were dramatically mitigated by 73.39% (dropping to 18.464 MW) accompanied by a +3.97% optimization in the network's average voltage profile; however, this technical enhancement incurred a severe 14.2% economic penalty, raising the hourly fuel cost to 154426.07 $/h due to a massive spatial re-dispatch from low-cost remote hubs to high-cost centralized nodes.

In summary, the unified framework successfully balances mathematical convexity, physical grid security, and market pricing transparency. Furthermore, the mathematical genericism of the proposed disaggregated reserve engine enables direct applicability to solar-integrated (PV-included) power systems. Unlike wind profile volatility, utility-scale PV plants introduce severe localized ramping stresses during solar-onset and sunset periods. By adjusting the uncertainty bounds within the stochastic dispatch layers, the proposed flexible ramping mechanism can efficiently secure non-simultaneous upward/downward ramping products specifically tailored to solar fluctuations, ensuring system reliability and precise nodal pricing signals under multi-renewable market environments. Future research trajectories will extend this linearized disaggregated architecture to encompass multi-period energy storage scheduling, dynamic network topology reconfiguration, and distribution-level transactive energy markets.

5 Acknowledgement

The authors would like to acknowledge the advanced computational facilities and academic guidance provided by the Faculty of Electrical Engineering at K. N. Toosi University of Technology.

Disclosure of Potential Conflicts of Interest

The Authors declare that there is no conflict of interest regarding the publication of this research article.

Reference

[1] A. J. Wood, B. F. Wollenberg, and G. B. Sheblé, *Power generation, operation, and control*. John wiley & sons, Sep., 2013.

[2] Z. Guo, J. Bai, S. Chen, and R. Wang, "Evaluating the Impact of Offering Prices on LMP: An Analytical Method," in *2025 7th Int. Conf. Power Energy Technol. (ICPET)*, Jul., 2025: IEEE, pp. 918-923, doi: https://doi.org/10.1109/ICPET66029.2025.11160418.

[3] L. A. Roald, D. Pozo, A. Papavasiliou, D. K. Molzahn, J. Kazempour, and A. Conejo, "Power systems optimization under uncertainty: A review of methods and applications," *Electr. Power Syst. Res.*, vol. 214, p. 108725, Jan., 2023, doi: https://doi.org/10.1016/j.epsr.2022.108725.

[4] R. Rezvanfar, K. Taghizad-Tavana, and M. T. Hagh, "A Comprehensive Review and Simulation-Based Analysis of Power Market Pricing Mechanisms in Energy Systems with High Penetration of Distributed Energy Resources: An Analysis of Distribution Locational Marginal Pricing, Dynamic Tariff, and Machine Learning-Based Approaches," *e-Prime Adv. Electr. Eng. Electron. Energy*, p. 101083, Sep., 2025, doi: https://doi.org/10.1016/j.prime.2025.101083.

[5] M. B. Cain, R. P. O'neill, and A. Castillo, "History of optimal power flow and formulations," *Fed. Energy Regul. Commission*, vol. 1, pp. 1-36, Dec., 2012.

[6] A. Babiker, S. S. Ahmad, I. Ahmed, M. Khalid, M. A. Abido, and F. S. Al-Ismail, "Optimal power flow: A review of state-of-the-art techniques and future perspectives," *IEEE Access*, Apr., 2025, doi: https://doi.org/10.1109/ACCESS.2025.3556168.

[7] H. Ergun, J. Dave, D. Van Hertem, and F. Geth, "Optimal power flow for AC–DC grids: Formulation, convex relaxation, linear approximation, and implementation," *IEEE Trans. Power Syst.*, vol. 34, no. 4, pp. 2980-2990, Feb., 2019, doi: https://doi.org/10.1109/TPWRS.2019.2897835.

[8] D. Shchetinin, T. T. De Rubira, and G. Hug, "On the construction of linear approximations of line flow constraints for AC optimal power flow," *IEEE Trans. Power Syst.*, vol. 34, no. 2, pp. 1182-1192, Oct., 2018, doi: https://doi.org/10.1109/TPWRS.2018.2874173.

[9] D. Jia, Z. Ren, and K. Liu, "Co-Optimization of Market and Grid Stability in High-Penetration Renewable Distribution Systems with Multi-Agent," *Energies*, vol. 18, no. 12, p. 3209, Jun., 2025, doi: https://doi.org/10.3390/en18123209.

[10] F. Capitanescu *et al.*, "State-of-the-art, challenges, and future trends in security constrained optimal power flow," *Electr. Power Syst. Res.*, vol. 81, no. 8, pp. 1731-1741, Aug., 2011, doi: https://doi.org/10.1016/j.epsr.2011.04.003.

[11] H. Chen, J. Huang, Z. Lin, F. Huang, and M. Li, "Stochastic economic dispatch based optimal market clearing strategy considering flexible ramping products under wind power uncertainties," *CSEE J. Power Energy Syst*, vol. 10, no. 4, pp. 1525-1535, Mar., 2023, doi: https://doi.org/10.17775/CSEEJPES.2021.06340.

[12] E. Ela, M. Milligan, and B. Kirby, "Operating reserves and variable generation," *Contract*, vol. 303, no. August, pp. 275-3000, Aug., 2011.

[13] H. Yuan, F. Li, Y. Wei, and J. Zhu, "Novel linearized power flow and linearized OPF models for active distribution networks with application in distribution LMP," *IEEE Trans. Smart Grid*, vol. 9, no. 1, pp. 438-448, Jul., 2016, doi: https://doi.org/10.1109/TSG.2016.2594814.

[14] Z. Wang, A. Younesi, M. V. Liu, G. C. Guo, and C. L. Anderson, "AC optimal power flow in power systems with renewable energy integration: A review of formulations and case studies," *IEEE Access*, vol. 11, pp. 102681-102712, Sep., 2023, doi: https://doi.org/10.1109/ACCESS.2023.3314330.

[15] R. D. Zimmerman, C. E. Murillo-Sánchez, and R. J. Thomas, "MATPOWER: Steady-state operations, planning, and analysis tools for power systems research and education," *IEEE Trans. Power Syst.*, vol. 26, no. 1, pp. 12-19, Jun., 2010, doi: https://doi.org/10.1109/TPWRS.2010.2051168.